Chaotic eigenfunctions in momentum space

A Bäcker and R Schubert

Abteilung Theoretische Physik, Universität Ulm, Albert-Einstein-Allee 11, D–89069 Ulm, Germany

E-mail: `baec@physik.uni-ulm.de` and `schub@physik.uni-ulm.de`

Abstract.   We study eigenstates of chaotic billiards in the momentum representation and propose the radially integrated momentum distribution as a useful measure to detect localization effects. For the momentum distribution, the radially integrated momentum distribution, and the angular integrated momentum distribution explicit formulae in terms of the normal derivative along the billiard boundary are derived. We present a detailed numerical study for the stadium and the cardioid billiard, which shows in several cases that the radially integrated momentum distribution is a good indicator of localized eigenstates, such as scars, or bouncing ball modes. We also find examples, where the localization is more strongly pronounced in position space than in momentum space, which we discuss in detail. Finally, applications and generalizations are discussed.

1. Introduction

In quantum mechanics the state of a system is given by a normalized vector in a Hilbert space, which in turn can be represented in different ways. Usually one chooses the representation which is most convenient for the problem at hand. In quantum chaos the main concern is to understand the semiclassical limit, and the fingerprints which properties of the classical limit, like chaoticity or integrability, leave on the quantum system.

A particulary convenient class of representations for the study of the quantum to classical correspondence is given by the Wigner function and its relatives, e.g. the Husimi density. The Wigner function of a quantum state is the representation which comes closest to a probability density on the phase space of the corresponding classical system [1, 2], and therefore should be a sensitive detector for classical fingerprints. One drawback of the Wigner function is that it is difficult to visualize, because it is a function on the $2n$-dimensional phase space. Therefore, one is often forced to study the projections on position or momentum space when one wants a visual representation of the state. Whereas the position representation is commonly used in quantum chaos, the momentum representation is not. Our aim here is to promote the momentum representation, by showing that it has some potential advantages.

What we are especially looking for are fingerprints of the classical phase space structure, e.g. periodic orbits. So in the position representation one is searching for an enhanced probability density around an orbit, in order to detect, for example, so-called scarred eigenstates [3]. But the detection of such a state from the probability density in position space can be rather ambiguous; there is no clear borderline which distinguishes scarred eigenstates from those which are not. In this case the probability density in momentum space can be helpful. For example, assume we are studying a Euclidean billiard system, where the periodic orbits consist of segments of straight lines; therefore the momentum distribution of a state which is

scarred by a periodic orbit should be concentrated on the directions of the line segments of that orbit. This criterion can be further simplified if one realizes that the momentum distribution of the nth state is concentrated on the energy shell $p^2 = E_n$, so that the main information is contained in the dependence on the direction of p. By integrating over the radial direction one gets a one-dimensional distribution, the angular distribution of the momentum, which contains all the essential information about the momentum distribution. This is the main advantage of the momentum representation, instead of working with a two-dimensional distribution as in position space, one can reduce the study to the one-dimensional angular distribution of the momentum.

A related quantity was introduced in [4], where the scattering approach is used to study expectation values and scars on the Poincaré section. The expectation values of a proposed 'scar operator' correspond to a smoothed angular distribution of the momentum. Other approaches to study eigenfunctions consist of the use of the Bargmann representation and the stellar representation [5]. For billiards, these can be used to obtain representations on the Poincaré section [6] (see also [7]).

The plan of this paper is as follows. In section 1 we use the boundary integral method to obtain expressions for the momentum representation of a given eigenfunction in terms of the normal derivative of this eigenfunction on the boundary. Furthermore, we derive formulae for the angular and the radial distribution of the momentum density, respectively, expressed in terms of the normal derivative. In section 2 we present a gallery of eigenstates displayed in position space and in momentum space, and compare the different representations. Finally, applications and generalizations are discussed.

2. Momentum distributions

The boundary integral method is a common method for computing eigenvalues and eigenfunctions of two-dimensional billiards, see e.g. [8, 9]. The main point is that one can reduce the two-dimensional eigenvalue problem in such a billiard with the help of Green's formula and a Green function into an integral equation for the normal derivative of the eigenfunction on the boundary. Therefore, one needs to solve only a one-dimensional problem, which is much more efficient numerically.

2.1. Reduction to the boundary

Let $\Omega \subset \mathbb{R}^2$ be a domain in the Euclidean plane with piecewise smooth boundary $\partial\Omega$. The Dirichlet quantum billiard in Ω is defined by

$$-\Delta\psi_n(q) = p_n^2\psi_n(q) \qquad \text{for} \quad q \in \Omega\backslash\partial\Omega \tag{1}$$

$$\psi_n(q) = 0 \qquad \text{for} \quad q \in \partial\Omega. \tag{2}$$

And we use the trivial extension of $\psi_n(q)$ to $\mathbb{R}^2$ by requiring $\psi_n(q) = 0$ for $q \in \mathbb{R}^2 \setminus \Omega$ to $\mathbb{R}^2$. The transformation of this problem to a problem on the boundary rests on the Green formula,

$$\int_\Omega [f(q)\Delta g(q) - g(q)\Delta f(q)]\,\mathrm{d}^2q$$
$$= \int_{\partial\Omega} [f(q(s))n(s)\nabla g(q(s)) - g(q(s))n(s)\nabla f(q(s))]\,\mathrm{d}s \tag{3}$$

where f and g are arbitrary smooth functions, and $n(s)$ denotes the outer normal on $\partial\Omega$, which is defined almost everywhere if the boundary is piecewise smooth. If one inserts for f a Green

function, e.g. $f(q) = -\frac{i}{4} H_0^{(1)}(p_n|q - q'|)$, where $H_0^{(1)} = J_0 + iY_0$ is the Hankel function of the first kind, which satisfies

$$(\Delta_q + p_n^2)\frac{-i}{4} H_0^{(1)}(p_n|q - q'|) = \delta(q - q') \tag{4}$$

and for g the eigenfunction ψ_n, one gets for $q \in \mathbb{R}^2 \setminus \partial\Omega$

$$\psi_n(q) = \int_{\partial\Omega} \frac{i}{4} H_0^{(1)}(p_n|q(s) - q|)u_n(s)\,\mathrm{d}s \tag{5}$$

where $u_n(s) := n(s)\nabla\psi_n(q(s))$ denotes the normal derivative of ψ_n on the boundary expressed in terms of the arclength coordinate s. Equation (5) is the crucial relation by which one recovers the eigenfunction from its normal derivative on the boundary. Taking the normal derivative of (5) leads to an integral equation for u_n on the boundary, which is then solved numerically. The choice of $H_0^{(1)}$ for the Green function is necessary in order that this integral equation for u_n does not lead to any spurious solutions, see e.g. [8]. For the integral (5) the contribution of J_0 is irrelevant, because with $(\Delta + p_n^2)J_0(p_n|q|) = 0$ the Green formula gives for $q \in \Omega \setminus \partial\Omega$

$$\int_{\partial\Omega} J_0(p_n|q(s) - q|)u_n(s)\,\mathrm{d}s = 0 \tag{6}$$

and so one has the simpler formula for the eigenfunction for $q \in \Omega \setminus \partial\Omega$

$$\psi_n(q) = -\frac{1}{4}\int_{\partial\Omega} Y_0(p_n|q(s) - q|)u_n(s)\,\mathrm{d}s. \tag{7}$$

Furthermore, one can express the L_2-norm of ψ_n by u_n as [9, 10]

$$\frac{1}{2p_n^2}\int_{\partial\Omega} n(s)q(s)|u_n(s)|^2\mathrm{d}s = ||\psi_n||^2. \tag{8}$$

This expression is very convenient as it allows one to obtain a normalized normal derivative u_n such that all other derived quantities of interest, such as expectation values, are correctly normalized. This relation is much faster to compute numerically than a normalization obtained from integrating $|\psi(q)|^2$ over the billiard domain Ω.

Even in cases where the eigenfunctions are given by an expansion into some basis it can be useful to perform the computations starting from the normal derivative, as one can exploit the relation (8) to obtain normalized eigenfunctions.

2.2. Momentum representation of eigenfunctions

The momentum representation of an eigenfunction ψ_n is given by its Fourier transform

$$\hat{\psi}_n(p) := \frac{1}{2\pi}\int_{\mathbb{R}^2} e^{-ipq}\psi_n(q)\,\mathrm{d}^2q = \frac{1}{2\pi}\int_\Omega e^{-ipq}\psi_n(q)\,\mathrm{d}^2q. \tag{9}$$

Using Green's formula (3) with $f(q) = \psi_n(q)$ and $g(q) = \frac{1}{2\pi}e^{-iqp}$ one gets

$$\frac{1}{2\pi}\int_\Omega [\psi_n(q)(-ip)^2 e^{-iqp} - e^{-iqp}(-p_n^2)\psi_n(q)]\,\mathrm{d}^2q$$

$$= \frac{1}{2\pi}\int_{\partial\Omega} [\psi_n(q(s))(-in(s)p)e^{-iq(s)p} - u_n(s)e^{-iq(s)p}]\,\mathrm{d}s. \tag{10}$$

As $\psi_n(q) = 0$ for $q \in \partial\Omega$, we get a representation of the Fourier transform as an integral over the normal derivative at the boundary

$$\hat{\psi}_n(p) = \frac{1}{p^2 - p_n^2}\frac{1}{2\pi}\int_{\partial\Omega} u_n(s)e^{-iq(s)p}\,\mathrm{d}s. \tag{11}$$

This expression has an apparent singularity at $p^2 = p_n^2$, but since the Fourier transform and its derivatives are bounded this singularity has to be cancelled by a zero of the integral. Solving (11) for the integral gives

$$\frac{1}{2\pi} \int_{\partial\Omega} u_n(s) e^{-iq(s)p} \, ds = (p^2 - p_n^2)\hat{\psi}_n(p) \tag{12}$$

and taking the derivative of this equation with respect to $r := |p|$ at the point $r = p_n$ one gets

$$\hat{\psi}_n(p) = -\frac{i}{4\pi p_n^2} \int_{\partial\Omega} e^{-ipq(s)} pq(s) u_n(s) \, ds \tag{13}$$

for $|p| = p_n$. By repeating this procedure one can get expressions for the derivatives of $\hat{\psi}_n(p)$ at $|p| = p_n$ as well. This can be used to interpolate near $|p| = p_n$ for a numerical plot of $\hat{\psi}_n(p)$.

2.3. Radially integrated momentum distribution

In a billiard the classical flows at different energies p^2 are isomorphic, because the system scales with energy. At the quantum mechanical side the momentum distribution of the nth state is concentrated around the energy shell $p^2 = p_n^2$. Because of the scaling property of the classical system the interesting phenomena, i.e. those which are due to the special system at hand, should occur only in the angular distribution of the momentum probability.

Therefore we want to study the angular distribution of the momentum defined by

$$I_n(\varphi) := \int_0^\infty |\hat{\psi}_n(r, \varphi)|^2 r \, dr \tag{14}$$

where we have introduced polar coordinates $p = (r\cos\varphi, r\sin\varphi)$. The advantage of this quantity, in contrast to the full momentum probability density or the probability distribution in position space, is that it depends only on one variable $\varphi \in [0, 2\pi]$.

By inserting the expression (11) for the Fourier transform $\hat{\psi}_n$ into (14) one gets

$$I_n(\varphi) = \frac{1}{(2\pi)^2} \int_0^\infty \frac{r}{(r^2 - p_n^2)^2} \iint_{\partial\Omega \times \partial\Omega} e^{-ir\alpha} u_n(s)\overline{u}_n(s') \, ds \, ds' \, dr \tag{15}$$

where we have used the abbreviation

$$\alpha = \alpha(\varphi, s, s') := \hat{p}(\varphi)(q(s) - q(s')) \tag{16}$$

and $\hat{p}(\varphi) = (\cos\varphi, \sin\varphi)$ is the unit vector in p direction. Using $\frac{r}{(r^2-p_n^2)^2} = -\frac{1}{2}\frac{d}{dr}\frac{1}{r^2-p_n^2}$ and partial integration one obtains

$$4\pi^2 I_n(\varphi) = -2\pi^2 p_n^2 |\hat{\psi}_n(0)|^2 - \frac{1}{2}\int_0^\infty \frac{1}{r^2 - p_n^2} \iint_{\partial\Omega \times \partial\Omega} i\alpha e^{-ir\alpha} u_n(s)\overline{u}_n(s') \, ds \, ds' \, dr \tag{17}$$

where it was used that $\int_{\partial\Omega} u_n(s) \, ds = -2\pi p_n^2 \hat{\psi}_n(0)$ which follows from (11).

Here we have to discuss a problem which always occurs when inserting the expression (11) for $\hat{\psi}_n$ in an integral such as in equation (14). Since (11) is the product of a factor which becomes singular at $|p| = p_n$ and a factor which is zero there, we have an apparent problem if we want to interchange the order of integration in (17). Therefore we choose a regularization for the factor $\frac{1}{p^2-p_n^2}$. This can be done by adding to p_n a small positive or negative imaginary part, $p_n \pm i\epsilon$, performing all computations and taking afterwards the limit $\epsilon \to 0$. The result

is independent of the regularization. In the following we choose a symmetric regularization, i.e., replace $(p^2 - p_n^2)^{-1}$ by

$$\frac{1}{2}\left(\frac{1}{p^2 - (p_n + i\epsilon)^2} + \frac{1}{p^2 - (p_n - i\epsilon)^2}\right) \tag{18}$$

which corresponds in the limit $\epsilon \to 0$ to taking the principal values of all integrals over $r = |p|$. To avoid complicated formulae we proceed formally without regularization, and interchange integrals whenever needed, but interpret all integrals over r as principal values. The reader can always check that the described regularization leads to the same results.

Returning to the computation of $I_n(\varphi)$ we interchange the order of integration in (17) and get

$$I_n(\varphi) = \iint_{\partial\Omega \times \partial\Omega} K_n(\varphi, s, s') u_n(s) \overline{u}_n(s') \, \mathrm{d}s \, \mathrm{d}s' \tag{19}$$

where the kernel is given by

$$K_n(\varphi, s, s') = -\frac{i\alpha}{8\pi^2} \int_0^\infty \frac{e^{-ir\alpha}}{r^2 - p_n^2} \, \mathrm{d}r - \frac{1}{2p_n^2}$$

$$= -\frac{\alpha}{8\pi^2} \int_0^\infty \frac{\sin(r\alpha)}{r^2 - p_n^2} \, \mathrm{d}r - \frac{1}{2p_n^2} - i\frac{\alpha}{8\pi^2} \int_0^\infty \frac{\cos(r\alpha)}{r^2 - p_n^2} \, \mathrm{d}r \tag{20}$$

and the integrals are interpreted as principal values. Note that the real part is an even function of α and the imaginary part is an odd function of α, thus K_n has the property

$$K_n(\varphi, s, s') = \overline{K}_n(\varphi, s', s) \tag{21}$$

which is equivalent to $\overline{I}_n(\varphi) = I_n(\varphi)$. For Euclidean billiards the eigenfunctions can be choosen to be real. In this case $\overline{u}_n(s)u_n(s')$ is even under interchange of s and s', and therefore the integral over the imaginary part of K_n, which is odd, vanishes.

From [11] one gets for the integrals (interpreted as principal values)

$$-\frac{\alpha}{8\pi^2} \int_0^\infty \frac{\sin(r\alpha)}{r^2 - p_n^2} \, \mathrm{d}r = \frac{1}{8\pi^2}(\sin(|\alpha|p_n)\,\mathrm{Ci}(|\alpha|p_n) - \cos(|\alpha|p_n)\,\mathrm{Si}(|\alpha|p_n)) \tag{22}$$

$$-\frac{\alpha}{8\pi^2} \int_0^\infty \frac{\cos(r\alpha)}{r^2 - p_n^2} \, \mathrm{d}r = \frac{\alpha}{16\pi p_n} \sin(|\alpha|p_n) \tag{23}$$

where Si and Ci denote the sine and cosine integrals. Note that for billiards with Dirichlet boundary conditions, $p_n > 0$. With the abbreviation

$$f(x) := \sin(x)\,\mathrm{Ci}(x) - \cos(x)\,\mathrm{Si}(x) \tag{24}$$

we can write our final expression for $I_n(\varphi)$ in terms of the normal derivative u_n as

$$I_n(\varphi) = \iint_{\partial\Omega \times \partial\Omega} \left[\frac{1}{8\pi^2} f(|\alpha|p_n) - \frac{1}{2p_n^2}\right] u_n(s)\overline{u}_n(s') \, \mathrm{d}s \, \mathrm{d}s'$$

$$+ i\iint_{\partial\Omega \times \partial\Omega} \frac{\alpha}{16\pi p_n} \sin(|\alpha|p_n) u_n(s)\overline{u}_n(s') \, \mathrm{d}s \, \mathrm{d}s'. \tag{25}$$

Recall that $\alpha = \alpha(\varphi, s, s') = \hat{p}(\varphi)(q(s) - q(s'))$. If the normal derivative u_n is real then the second term in (25) vanishes, and if furthermore the eigenfunction ψ_n is odd with respect to some discrete symmetry of the billiard, see the appendix, then $\int_{\partial\Omega} u_n(s) \, \mathrm{d}s = 0$. So under these special conditions the expression (25) simplifies to

$$I_n(\varphi) = \frac{1}{8\pi^2} \iint_{\partial\Omega \times \partial\Omega} f(|\alpha|p_n) u_n(s) u_n(s') \, \mathrm{d}s \, \mathrm{d}s'. \tag{26}$$

2.4. Angular integrated momentum density

Similarly to the radially integrated momentum density one can study the radial distribution of the momentum density by integrating over the angle φ. The radial momentum distribution is defined as

$$R_n(r) := r \int_0^{2\pi} |\hat{\psi}_n(r, \varphi)|^2 \, \mathrm{d}\varphi \tag{27}$$

and if we insert the expression (11) for $\hat{\psi}_n$ one gets

$$R_n(r) := \frac{r}{(r^2 - p_n^2)^2} \frac{1}{(2\pi)^2} \iint_{\partial\Omega \times \partial\Omega} u_n(s)\overline{u}_n(s') \int_0^{2\pi} \mathrm{e}^{-\mathrm{i}|q(s)-q(s')|r\cos(\varphi)} \, \mathrm{d}\varphi \, \mathrm{d}s \, \mathrm{d}s'$$

$$= \frac{r}{(r^2 - p_n^2)^2} \frac{1}{2\pi} \iint_{\partial\Omega \times \partial\Omega} u_n(s)\overline{u}_n(s') J_0(|q(s) - q(s')|r) \, \mathrm{d}s \, \mathrm{d}s'. \tag{28}$$

Again one has an apparent singularity at $r = p_n$ due to the pre-factor $1/(r^2 - p_n^2)^2$. In the same way as in the previous section, by differentiating $(r^2 - p_n^2)^2 R_n(r)/r$ sufficiently often one obtains

$$R_n(p_n) = \frac{1}{8p_n} \left(\frac{\mathrm{d}}{\mathrm{d}r}\right)^2 \left((r^2 - p_n^2)^2 \frac{R_n(r)}{r}\right)_{r=p_n} \tag{29}$$

$$R_n'(p_n) = \frac{1}{24p_n} \left(\frac{\mathrm{d}}{\mathrm{d}r}\right)^3 \left((r^2 - p_n^2)^2 \frac{R_n(r)}{r}\right)_{r=p_n} \tag{30}$$

and higher derivatives of R_n at $r = p_n$ can be obtained in the same way. Using equation (28) one gets

$$R_n(p_n) = \frac{1}{16\pi p_n} \iint_{\partial\Omega \times \partial\Omega} u_n(s)\overline{u}_n(s')|q(s) - q(s')|^2$$

$$\times \tfrac{1}{2}[J_2(|q(s) - q(s')|r) - J_0(|q(s) - q(s')|r)] \, \mathrm{d}s \, \mathrm{d}s' \tag{31}$$

$$R_n'(p_n) = \frac{1}{48\pi p_n} \iint_{\partial\Omega \times \partial\Omega} u_n(s)\overline{u}_n(s')|q(s) - q(s')|^3$$

$$\times \tfrac{1}{4}[3J_1(|q(s) - q(s')|r) - J_3(|q(s) - q(s')|r)] \, \mathrm{d}s \, \mathrm{d}s' \tag{32}$$

and these expressions can be used to interpolate in the region around $r = p_n$.

3. Gallery of eigenfunctions in momentum space

In the following we present a number of examples of eigenfunctions in momentum representation for two chaotic billiards and compare them with the position representation. A series of eigenfunctions of the cosine billiard in momentum representation can be found in [12]. The first system we study is the stadium billiard, which is proven to be strongly chaotic, i.e. it is ergodic, mixing and a K-system [13, 14]. The height of the desymmetrized billiard is chosen to be 1, and a denotes the length of the upper horizontal line, for which we have $a = 1.8$ in the following. To compare the structures in the eigenfunctions with the classical orbits, we use the symbolic dynamics proposed in [15], which is proven in [16].

The second system is the cardioid billiard, which is the limiting case of a family of billiards introduced in [17]. The cardioid billiard is proven to be ergodic, mixing, a K-system and a Bernoulli system [18–20]. The eigenvalues of the cardioid billiard have been provided by

Prosen and Robnik [21] and were calculated by means of the conformal mapping technique, see e.g. [22, 23]. To describe the periodic orbits in the cardioid we use the symbolic dynamics proposed in [24, 25], see [16, 26] for proofs.

As these two billiards are ergodic, the quantum ergodicity theorem [27–31] applies, see e.g. [32–34] for introductions. It implies that for 'almost all' eigenfunctions their Wigner functions $W_n(p, q)$ become equidistributed on the energy shell in the semiclassical limit, i.e.

$$W_{n_j}(p, q) := \int_{\mathbb{R}^2} e^{iq'p} \overline{\psi}_{n_j}\left(q - \frac{q'}{2}\right) \psi_{n_j}\left(q + \frac{q'}{2}\right) d^2q' \sim \frac{\delta(p^2 - E_{n_j})}{\text{vol}(\Sigma_{E_{n_j}})} \tag{33}$$

where $\text{vol}(\Sigma_E) = \iint_{\mathbb{R}^2 \times \Omega} \delta(p^2 - E) d^2p \, d^2q$ is the volume of the energy shell. 'Almost all' precisely means that equation (33) holds for a subsequence $\{n_j\} \subset \mathbb{N}$ of density one, that is one has

$$\lim_{E \to \infty} \frac{\#\{n_j | E_{n_j} < E\}}{\#\{n | E_n < E\}} = 1. \tag{34}$$

For the eigenstates in position and momentum representation the quantum ergodicity theorem implies that

$$|\psi_{n_j}(q)|^2 \to \frac{1}{\text{vol}(\Omega)} \qquad \text{as} \quad n_j \to \infty \tag{35}$$

and

$$|\hat{\psi}_{n_j}(p)|^2 \to \frac{1}{\pi} \delta(p^2 - E_{n_j}) \qquad \text{as} \quad n_j \to \infty \tag{36}$$

in the weak sense. For the radially integrated momentum distribution it follows that

$$I_{n_j}(\varphi) \to \frac{1}{2\pi} \qquad \text{as} \quad n_j \to \infty \tag{37}$$

in the weak sense. For the angular integrated momentum density one has, in general, independent of the ergodic properties of the classical system,

$$R_{n_j}(r) \to 2r\delta(r^2 - E_{n_j}) \qquad \text{as} \quad n_j \to \infty. \tag{38}$$

Of special interest are, of course, the subsequences of exceptional eigenfunctions (if they exist) which are, according to the quantum ergodicity theorem, of density zero for ergodic systems. A drastic example of such eigenfunctions are the so-called bouncing ball modes in the stadium (which also occur in other billiards with two parallel walls). These eigenfunctions localize on the orbits which bounce up and down between the two parallel walls with perpendicular reflections at the boundary. For the stadium billiard the counting function for these modes increases asymptotically as $E^{3/4}$ [35, 36].

Another important class of exceptional eigenfunctions are the so-called 'scarred' eigenfunctions [3], showing localization along unstable periodic orbits, which were first observed in the stadium billiard. Scarred eigenfunctions have also been observed in the cardioid billiard [34, 37]. As was mentioned in the introduction, for an eigenfunction which is scarred by a periodic orbit, $I_n(\varphi)$ should have prominent peaks at the angles corresponding to the directions of the orbit, whose intensity is expected to be proportional to the length of the corresponding orbit segment.

Let us start the discussion by showing plots of some low-lying eigenfunctions of the stadium billiard with odd–odd symmetry. Figures 1 and 2 show, for the stadium billiard, three-dimensional plots of $|\psi_n(q)|^2$, $|\hat{\psi}_n(p)|^2$ and the corresponding greyscale plots. Furthermore, $I_n(\varphi)$ and $R_n(r)$ are shown. In the case of $I_n(\varphi)$ we only plot the interval $\varphi \in [0, \pi/2]$, as the other directions are obtained from symmetry, e.g. $I_n(\varphi) = I_n(\pi - \varphi)$ for $\varphi \in [\pi/2, \pi]$.
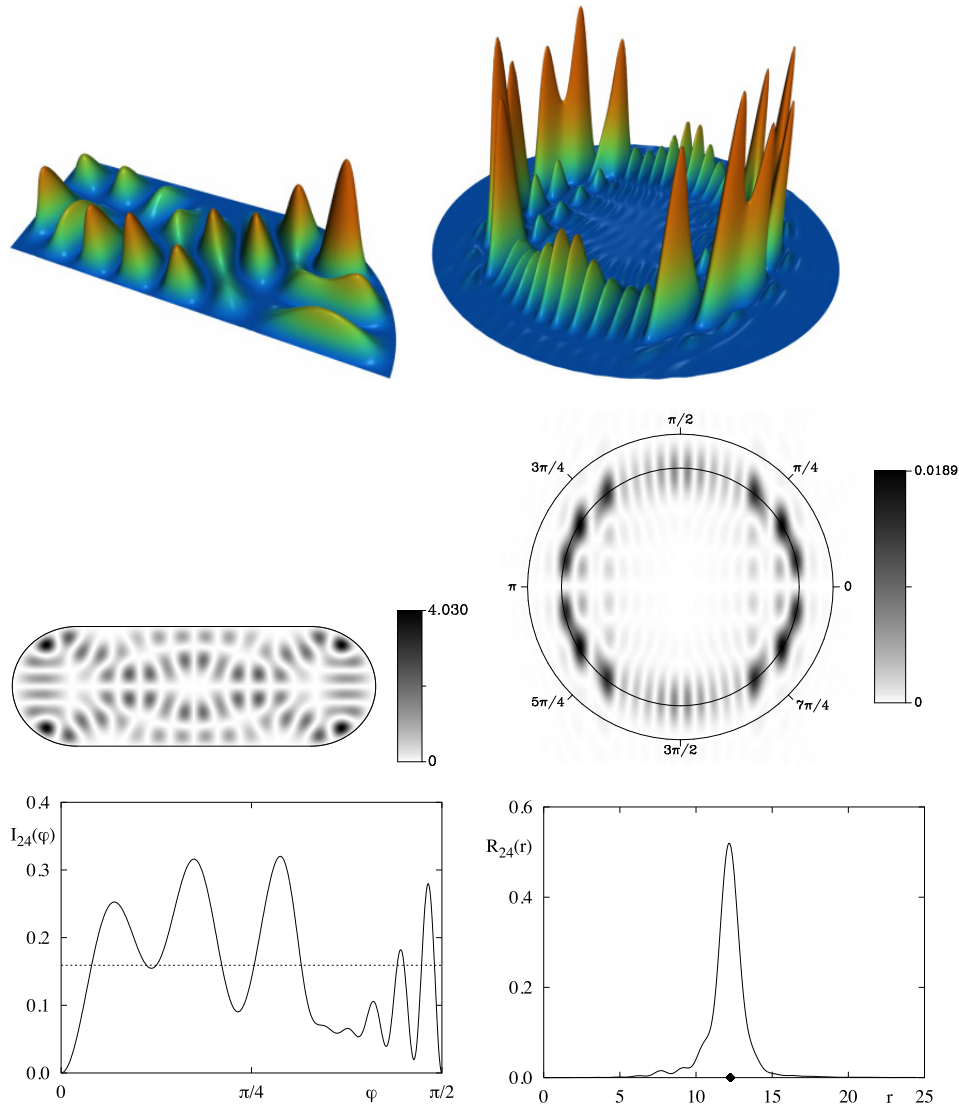
Figure 1. For $n = 24$, odd–odd symmetry: three-dimensional plots of $|\psi_{24}(q)|^2$, $|\hat{\psi}_{24}(p)|^2$, their corresponding greyscale pictures and the plot of the radially integrated momentum distribution $I_{24}(\varphi)$ and the angular integrated momentum distribution $R_{24}(r)$. The momentum distribution $|\hat{\psi}_{24}(p)|^2$ is concentrated around the energy shell, which is indicated as the inner circle. This is also clearly visible in the plot of $R_{24}(r)$. The angular distribution $I_{24}(\varphi)$ does not show any significantly preferred directions and the plot of $|\psi_{24}(q)|^2$ also does not show any prominent patterns.

The dashed line in the plot of $I_n(\varphi)$ corresponds to the mean value $1/(2\pi)$, see equation (37). The state $n = 24$ displayed in figure 1 does not show any prominent localization in position space, whereas the state $n = 26$, figure 2, is an example of a low-lying bouncing ball mode. For both eigenstates the momentum distribution $|\hat{\psi}_n(p)|^2$ is mainly concentrated around the energy shell $E_n = p^2$, which is indicated by the inner full circle in figures 1 and 2. This is also nicely seen in the plots of $R_{24}(r)$ and $R_{26}(r)$ where the radius of the energy shell is marked by
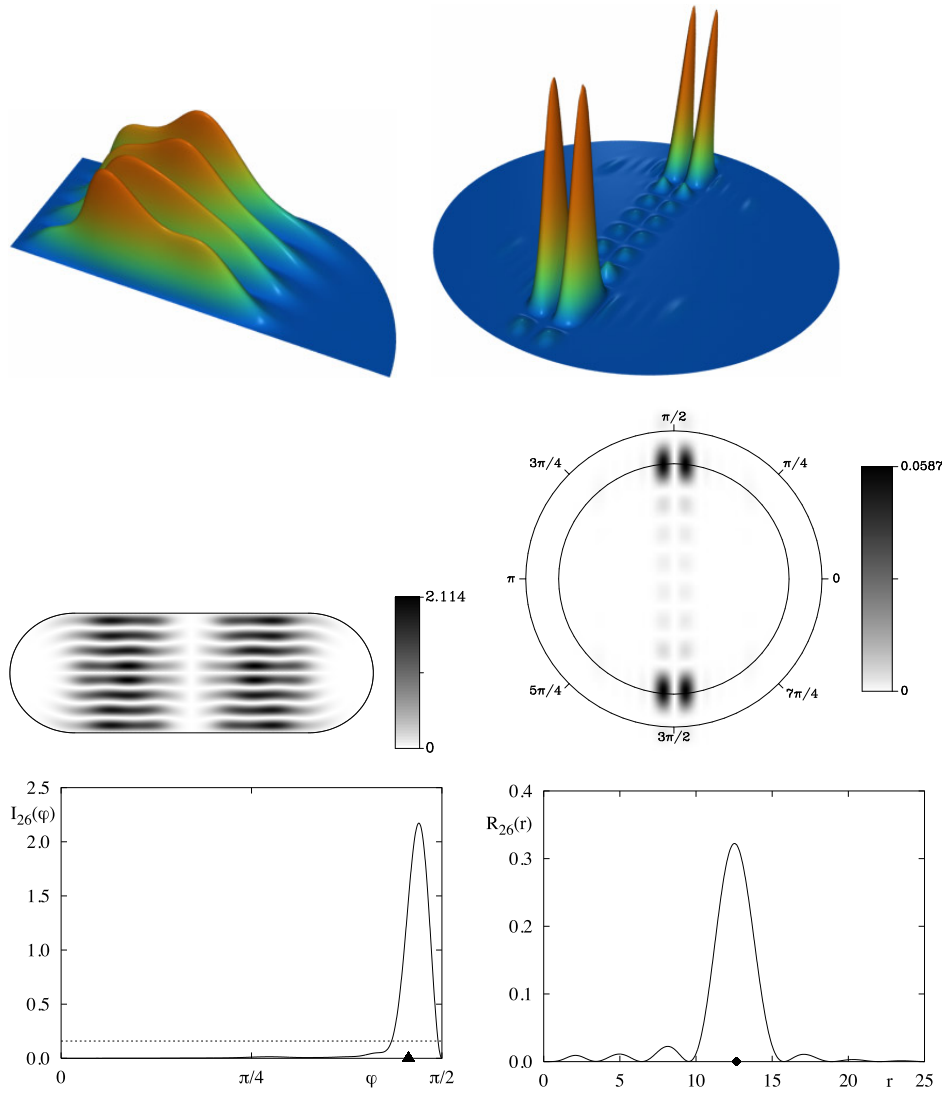
Figure 2. For $n = 26$, odd–odd symmetry: an example of a low-lying bouncing ball mode, for which $|\psi_{26}(q)|^2$ is localized on the rectangular part of the billiard. The plot of the momentum distribution $|\hat{\psi}_{26}(p)|^2$ shows a strong localization in the momentum directions ($p_x \approx 0$, $p_y \approx \pm p_n$) of the bouncing ball orbits. This is also clearly seen in the plot of $I_{26}(\varphi)$, which is concentrated near to $\varphi = \pi/2$. The corresponding direction $\varphi_{2,8}^{\text{bb}} = \arctan(4a)$ is marked by a triangle. In the plot of $R_{26}(r)$ one observes some additional oscillations in comparison with $R_{24}(r)$ in figure 1.

a rhombus. Whereas $|\hat{\psi}_{24}(p)|^2$ shows peaks at several places, $|\hat{\psi}_{26}(p)|^2$ only has prominent peaks around the p_y direction. The pictures shown in figure 2 are precisely those expected for a bouncing ball mode [36]: in position space we have localization on the rectangular part of the billiard, and in momentum space there is localization in the direction of the bouncing ball orbits. That there are four major peaks of $|\hat{\psi}_{26}(p)|^2$ visible in figure 2 is due to the symmetry of the billiard, which implies that $|\hat{\psi}_n(p)|^2$ is reflection symmetric with respect to the axes $p_x = 0$ and $p_y = 0$, on which $|\hat{\psi}_n(p)|^2$ vanishes for the stadium billiard with everywhere
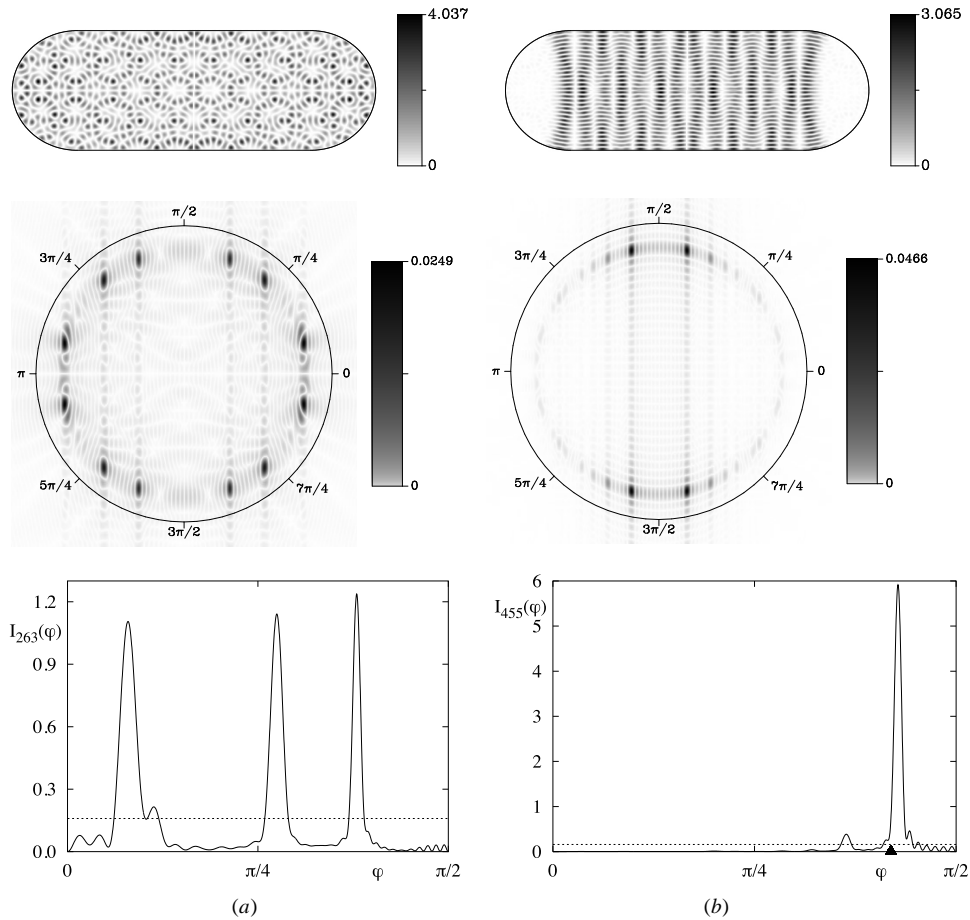
Figure 3. (*a*) $n = 263$, odd–odd symmetry; (*b*) $n = 455$, odd–odd symmetry. In (*a*) an example of an eigenfunction is shown which appears to be completely non-localized in position space. However, in momentum space $|\hat{\psi}_{263}(\boldsymbol{p})|^2$ and $I_{263}(\varphi)$ show clear localization in three major momentum directions. The second eigenfunction is an example of a higher-lying bouncing ball mode with 14 modes in the x-direction and 30 modes in the y-direction. Consequently, the corresponding momentum distributions show localization near to the $\varphi = \pi/2$ direction. In the plot of $I_{455}(\varphi)$ the triangle marks the direction $\varphi^{\text{bb}}_{14,30} = \arctan(\frac{30}{14}a)$.

Dirichlet boundary conditions. According to [36] the peaks should be in the directions

$$\pm\varphi^{\text{bb}}_{k,l} \qquad \text{and} \qquad \pi \pm \varphi^{\text{bb}}_{k,l} \qquad \text{with} \quad \varphi^{\text{bb}}_{k,l} := \arctan(al/k) \tag{39}$$

where k denotes the number of modes in the x-direction and l denotes the number of modes in the y-direction and $a = 1.8$ is the billiard parameter. If the ratio l/k increases, then the value of $\varphi^{\text{bb}}_{k,l}$ increases, and in the limit $l/k \to \infty$ we have $\varphi^{\text{bb}}_{k,l} \to \pi/2$. For the bouncing ball mode shown in figure 2 there is good agreement with the direction $\varphi^{\text{bb}}_{2,8} = \arctan(4a)$, which is marked by a full triangle in the plot of $I_{26}(\varphi)$.

Figure 3(*a*) shows an example of an eigenfunction having quite a regular and uniform pattern in position space. However, the plots of $|\hat{\psi}_{263}(\boldsymbol{p})|^2$ and $I_{263}(\varphi)$ reveal three major momentum directions. Although we did not succeed to find an orbit corresponding to these directions, there is some indication that this orbit should have quite a large geometric length.
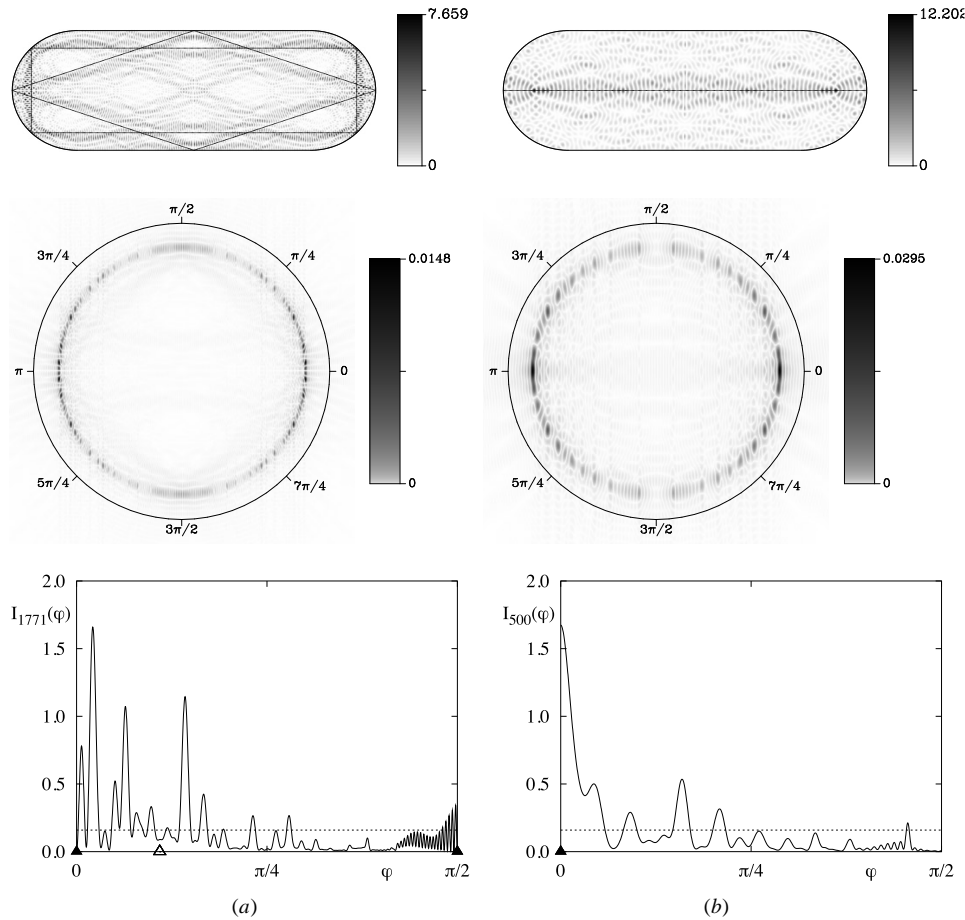
Figure 4. (*a*) $n = 1771$, odd–odd symmetry; (*b*) $n = 500$, even–even symmetry. In (*a*) the eigenfunction shows localization along the $\overline{1155}$ orbit of rectangular shape and also the $\overline{0123}$ orbit in the stadium. In the plot of $I_{1771}(\varphi)$ the corresponding momentum directions are marked by full triangles ($\overline{1155}$ orbit) and open triangles ($\overline{0123}$ orbit). The state $n = 500$ of even–even symmetry provides a nice example of an eigenfunction localized around the shortest unstable orbit, which runs along the symmetry axis. This is also seen in the plots of $|\hat{\psi}_{500}(\boldsymbol{p})|^2$ and $I_{500}(\varphi)$, which show a strong enhancement in the $\varphi = 0, \pi$ directions.

The second eigenfunction shown in figure 3 is an example of a higher-lying bouncing ball mode with 14 modes in the *x*-direction and 30 modes in the *y*-direction. For this bouncing ball mode the distance of the maximum to these directions is larger than for the one displayed in figure 2. This is well accounted for by the formula (39), as the location of the maximum of $I_{455}(\varphi)$ is close to $\varphi_{14,30}^{\mathrm{bb}} = \arctan(30/14a)$, which is marked by a full triangle in the plot of $I_{455}(\varphi)$.

Figure 4 shows two examples of eigenfunctions showing scarred structures in position space. $|\psi_{1771}(\boldsymbol{q})|^2$ shows an enhanced probability along the two orbits with symbolic codes $\overline{0123}$ for the orbit of diamond shape, and $\overline{1155}$ for the orbit of rectangular shape (shown as dashed lines in the plot of $|\psi_{1771}(\boldsymbol{q})|^2$). These two structures are less visible in the momentum representations. For the contribution of the diamond orbit to $I_{1771}(\varphi)$ we find that it is spread out near to $\varphi = \pi/8$, in agreement with the structure in position space, which is also not
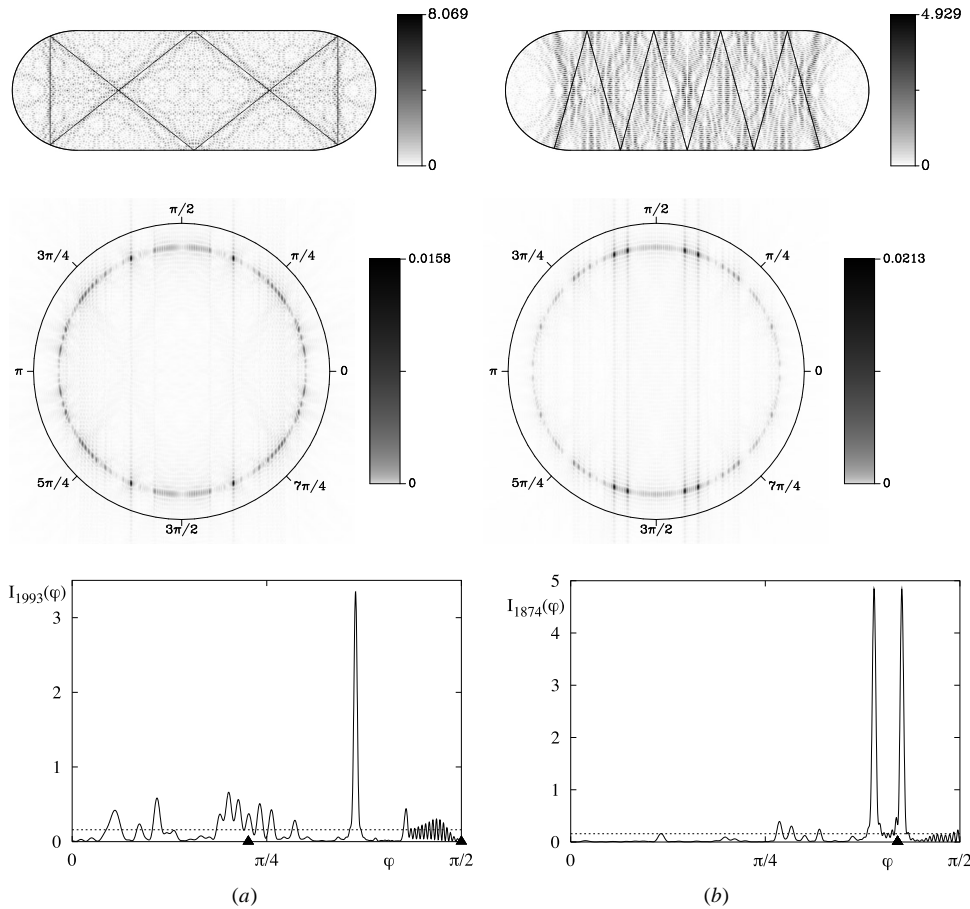
Figure 5. (*a*) $n = 1993$, even–even symmetry; (*b*) $n = 1874$, odd–odd symmetry. The eigenfunction in (*a*) is localized in position space along the $\overline{1105552}$ orbit. This orbit has two different momentum directions (in the interval $\varphi \in [0, \pi/2]$), still there is an additional high peak visible for $I_{1993}(\varphi)$. This illustrates that, for $I_n(\varphi)$, not just the height of the peak is relevant, but the total area below a peak, which accounts for a high probability in the corresponding direction. In (*b*) an example of an eigenfunction is shown, which is localized on the rectangular part of the stadium billiard, but which is not a bouncing ball mode. This eigenfunction may be understood in terms of the plotted orbit, although in momentum space there are additional prominent momentum directions. This might indicate that other orbits also contribute to the eigenfunction, see the text for further discussion.

aligned precisely along the diamond orbit. The higher intensity near to $\varphi = 0$ corresponds to localization along the rectangular orbit. Although $|\psi_{1771}(\boldsymbol{q})|^2$ shows stronger localization near to the circular boundary which seems to be associated with the $\varphi = \pm\pi/2$ directions, there is no prominent peak in that direction. However, there is some enhancement of the total probability to find the particle with momentum directions $3\pi/8 < \varphi < \pi/2$ which is seen more clearly in the plot of $|\hat{\psi}_{1771}(\boldsymbol{p})|^2$ than in the plot of $I_{1771}(\varphi)$. The rapid oscillations of $I_{1771}(\varphi)$ near to $\varphi = \pi/2$ are not a numerical artefact; the structures are also visible in the plot of $|\hat{\psi}_{1771}(\boldsymbol{p})|^2$; we will return to this point at the end of this section. In figure 4(*b*) an eigenfunction with clear localization in position space is shown, this time for the stadium billiard with even–even symmetry. The eigenfunction $\psi_{500}(\boldsymbol{q})$ shows localization along the

unstable $\overline{01}$ orbit running along the symmetry axis. This localization is also clearly seen in momentum space, where $|\hat{\psi}_{500}(\boldsymbol{p})|^2$ shows strong enhancement in the directions $\varphi = 0, \pi$, corresponding to a strong peak of $I_{500}(\varphi)$ at $\varphi = 0$.

Figure 5 shows two further examples of localized eigenfunctions. The eigenfunction with $n = 1993$ displayed in figure 5(*b*) shows clear localization in position space along the $\overline{110552}$ orbit. In momentum space there is one significant momentum direction at $\varphi \approx 3\pi/8$; however, this direction does not correspond to the pattern seen in position space, from which one would expect an important contribution to $|\hat{\psi}_{1993}(\boldsymbol{p})|^2$ and $I_{1993}(\varphi)$ in the direction of $\varphi = 0.71\ldots$. Indeed near to this direction there is a range of angles for which $I_{1993}(\varphi)$ has a number of smaller peaks, which together lead to an enhanced probability in this interval compared with other intervals. This example again illustrates that not just the height of the peaks is of importance in the interpretation of the pictures for $I_n(\varphi)$, but the overall accumulated probability corresponding to some interval of momentum directions.

In [34] the rate of quantum ergodicity has been studied both in position and in momentum space. For the stadium billiard it was expected that if the bouncing ball modes are the dominating (in the sense of having the strongest increase in the counting function) subsequence of localized eigenfunctions, that then the rate of quantum ergodicity should obey $S_1(E, A) := \frac{1}{N(E)} \sum_{E_n \leqslant E} |\langle \psi_n, A\psi_n \rangle - \overline{\sigma(A)}| \sim E^{-1/4}$. However, it turned out that the rate is much slower [34], at least in the considered energy range covering the first 6000 eigenfunctions. This was attributed to a considerable number of eigenfunctions, which show localization in position space in the rectangular part of the billiard, without being bouncing ball modes, see figure 11 of [34]. One example is shown in figure 5(*b*). One sees that they are also localized in momentum space near the direction $\varphi = \pi/2$, like the bouncing ball modes, but have more peaks. These states seem to correspond to the set of periodic orbits which are bouncing m times between the parallel walls before they are reflected into themselves in the circular part. One of them, the $\overline{2020202320202024}$ orbit, is shown in the density plot of $|\psi_{1874}(\boldsymbol{q})|^2$. Since the lengths of these orbits for large m are close to being rationally dependent one can speculate, that the naive Bohr–Sommerfeld quantization leads to a number of eigenvalue sequences which have some very close pairs of eigenvalues, for which the corresponding eigenfunction should be scarred by the corresponding orbits. The plot $I_{1874}(\varphi)$ indicates that this happens, because it has strong peaks at the directions corresponding to two orbits.

The cardioid billiard possesses no parallel walls and therefore no bouncing ball modes; in this sense it is more generic than the stadium billiard. Figure 6 shows for the cardioid billiard three-dimensional plots of $|\psi_{24}(\boldsymbol{q})|^2$, $|\hat{\psi}_{24}(\boldsymbol{p})|^2$ and the corresponding greyscale plots. Furthermore, $I_{24}(\varphi)$ and $R_{24}(r)$ are shown. This eigenstate of odd symmetry shows localization in position space around the unstable orbit $\overline{AB}$, which is also indicated in the plot. This localization is also reflected in the plots of $|\hat{\psi}_{24}(\boldsymbol{p})|^2$ and $I_{24}(\varphi)$. In the plot of $I_{24}(\varphi)$ the corresponding momentum direction of the orbit is marked by a full triangle at $\varphi = \pi/2$. At this place one observes a local minimum of $I_{24}(\varphi)$, but overall there is a large intensity near to $\varphi = \pi/2$. The plot of $R_{24}(r)$ shows the expected localization (plus some oscillations) around the energy shell $r = |\boldsymbol{p}_n|$, indicated by the rhombus. In the plots of the Fourier transforms the energy shell is marked by the full inner circle.

In figure 7, the first example shows clear localization in position space along the orbit with code $\overline{AAABBB}$. In momentum space, a neighbourhood of the vertical direction ($\varphi = \pi/2$) shows an enhanced probability, whereas the second direction, $\varphi = 0.62\ldots$, is not as prominent as one might expect from the picture of the eigenfunction in position space. The second eigenfunction shown in figure 7 is an example of a non-localized eigenfunction, which is also nicely seen in the plots of the momentum distributions, which do not show any preferred momentum direction.
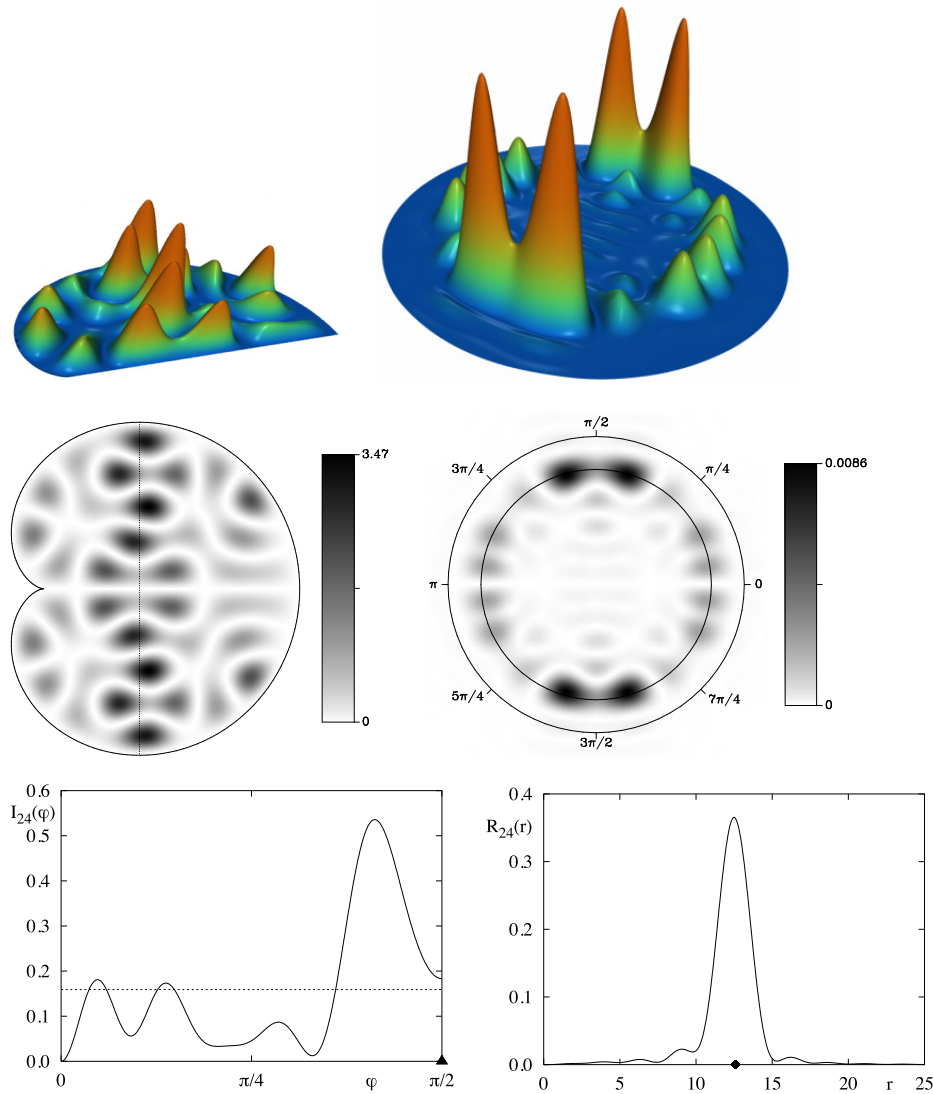
Figure 6. For $n = 1$, odd symmetry: three-dimensional plots of $|\psi_{24}(q)|^2$, $|\hat{\psi}_{24}(p)|^2$, their corresponding greyscale pictures and the plot of the radially integrated momentum distribution $I_{24}(\varphi)$ and the angular integrated momentum distribution $R_{24}(r)$. The momentum distribution $|\hat{\psi}_{24}(p)|^2$ is concentrated around the energy shell, which is indicated by the inner circle. This is also clearly visible in the plot of $R_{24}(r)$. Furthermore, this state is to some extent localized along the $\overline{AB}$ orbit, leading to an enhancement of $|\hat{\psi}_{24}(p)|^2$ near to $\varphi = \pi/2$, $3\pi/2$, also seen in the plot of $I_{24}(\varphi)$ near to the momentum direction $\varphi = \pi/2$ (marked by a triangle).

Figure 8(*a*) shows an example an of eigenfunction localized along the $\overline{AB}$ orbit, which is clearly seen in the plot of $|\psi_{1817}(q)|^2$. A similar eigenfunction, $\psi_{2605}(q)$, was found in [38] to have the largest maximum norm $||\psi_n||_\infty$ among the first 6000 eigenfunctions of odd symmetry. Also, the corresponding momentum distribution reveals that the direction $\varphi = \pi/2$ stands out. The second eigenfunction in figure 8(*b*) shows localization along the cusp orbit $CAAC$, and thus is an example of an *diffractive scar*. However, this localization is not reflected in

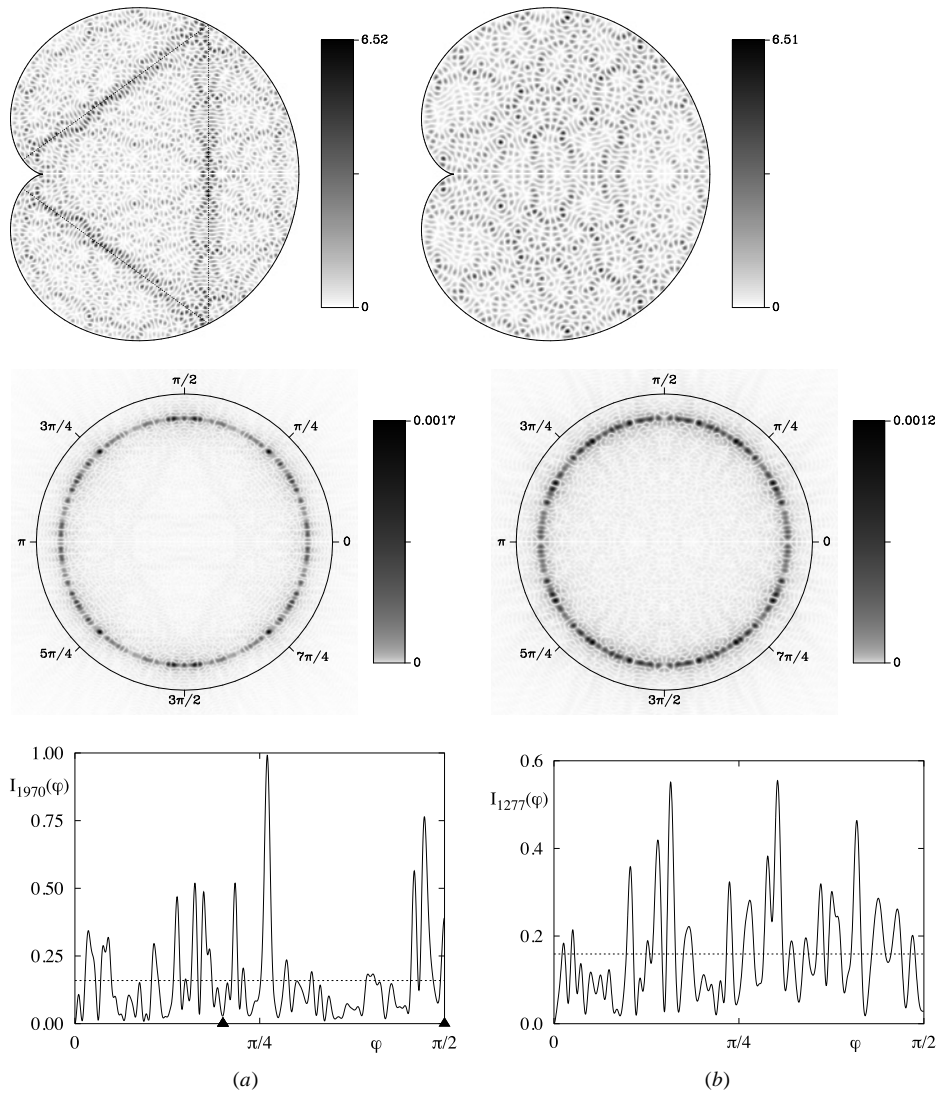**Figure 7.** (*a*) $n = 1970$, odd symmetry; (*b*) $n = 1277$, odd symmetry. The eigenfunction in (*a*) shows localization along the $\overline{AAABBB}$ orbit. There is some enhancement in the corresponding momentum directions, in particular near $\varphi = \pi/2$, and less significantly for the second direction near $\pi/4$. The eigenfunction in (*b*) is an example which appears to be quite delocalized both in position and in momentum space. The pictures look like those expected, according to the quantum ergodicity theorem, for a typical eigenfunction.

an enhancement of the momentum distribution in the corresponding directions. This may correspond to the fact that the enhancement is also not very strong in position space and nor precisely around the cusp orbit.

We conclude our survey of eigenfunctions in momentum space with two further examples of localized eigenfunctions. For the first example in figure 9(*a*) one observes that $|\psi_{1538}(\boldsymbol{q})|^2$ is clearly localized along the billiard boundary. Due to the non-convexity of the billiard there are no whispering gallery orbits as in the stadium billard. However, as found in [25], in the cardioid
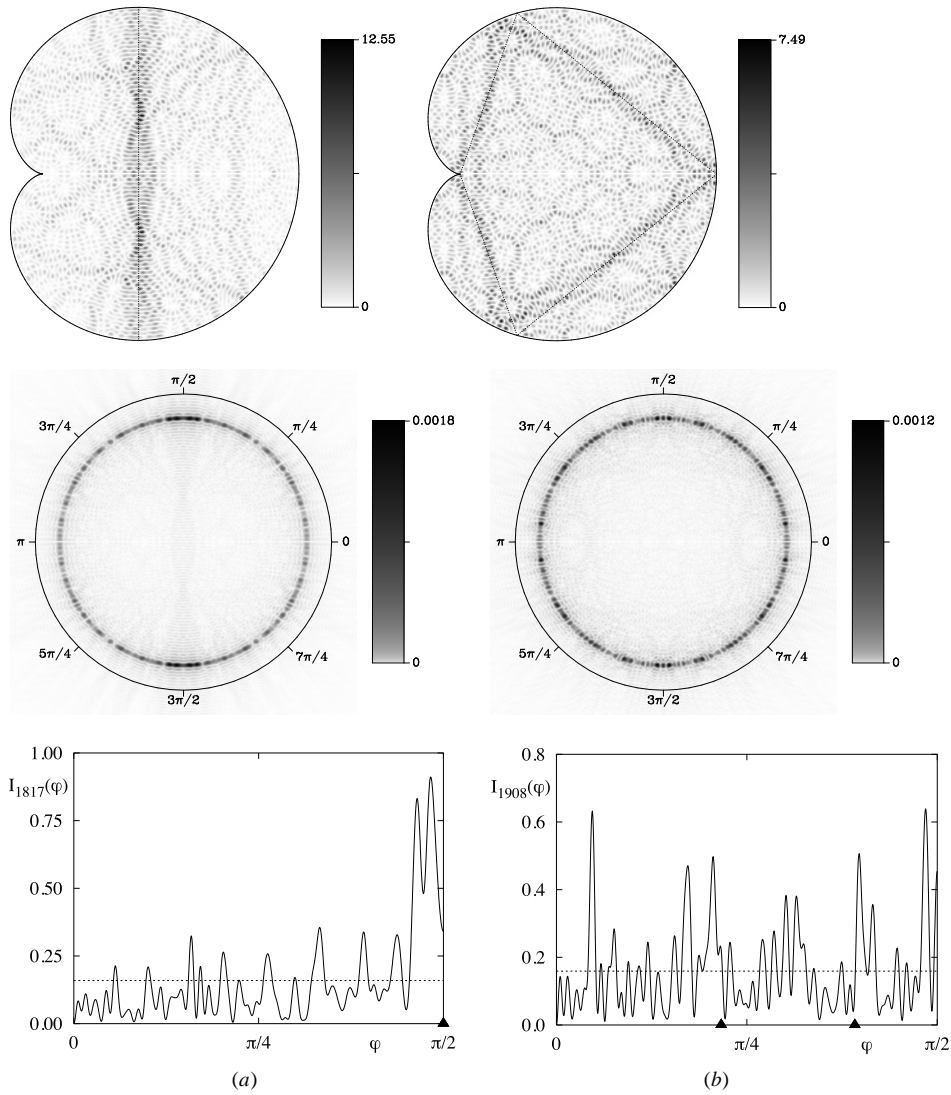
Figure 8. (*a*) $n = 1817$, odd symmetry; (*b*) $n = 1908$, odd symmetry. In (*a*) an example of an eigenfunction localized along the $\overline{AB}$ orbit is shown, which is also reflected in the corresponding momentum distribution. The eigenfunction displayed in (*b*) shows localization along the cusp orbit $CAAC$, and thus is an example of a *diffractive scar*. The association of the corresponding momentum directions seems to be ambiguous.

there exist families of periodic orbits which accumulate in length. A candidate responsible for the structure visible in $|\psi_{1538}(q)|^2$ is the family of orbits with code $\overline{A^n BABB}$. This type of orbit also accounts for the additional structures visible in the interior of the billiard. As for an orbit running along the boundary, all momentum directions occur; one expects to see only the two further directions of the part of the orbit inside the billiard, which are marked by triangles in the plot of $I_{1538}(\varphi)$. The second eigenfunction in figure 9(*b*) is localized along the $\overline{AABB}$ orbit, which is also seen in the corresponding momentum distributions. Near to the symmetry axis $|\psi_{1252}(q)|^2$ the enhanced region is much larger, presumably due to interference effects.
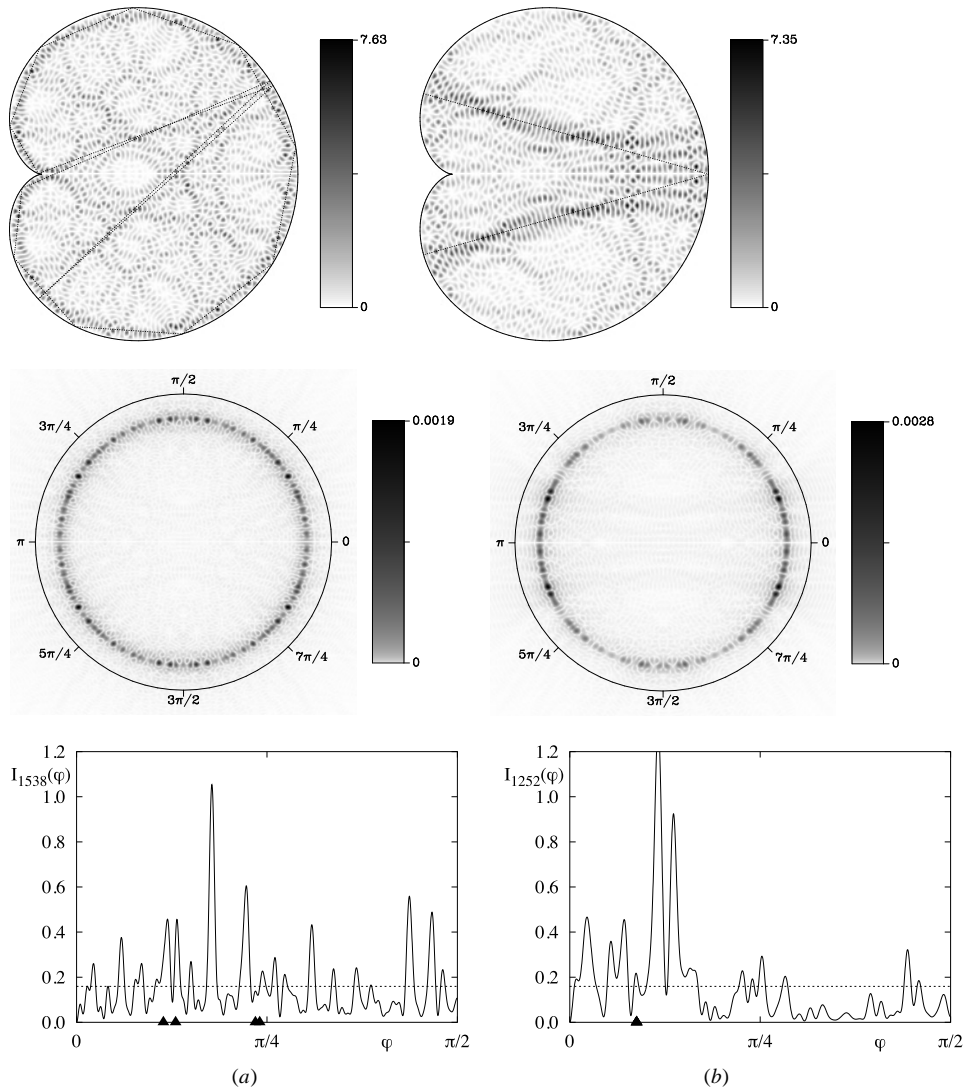
Figure 9. (a) $n = 1538$, odd symmetry; (b) $n = 1252$, odd symmetry. The eigenfunction displayed in (a) is mainly localized along the boundary. The family of orbits with code $\overline{A^n BABB}$ appears to describe the observed pattern quite well. In the plot of $I_{1538}(\varphi)$ only the momentum directions of the part of the orbit running inside the billiard are marked by triangles. The second example shows a nice example of an eigenfunction showing scarring along the $\overline{AABB}$ orbit is shown. Near to the symmetry axis the eigenfunction density is spread out. In momentum space there is a clear enhancement, which is close to (although not as close as one might expect) the momentum direction of the orbit.

For the cardioid billiard one generally observes a finer scale on which $I_n(\varphi)$ fluctuates, compared with the stadium billiard. For the stadium billiard the momentum distributions are stretched in the p_y direction, due to the long parallel segments of the boundary. This leads to the effect that the radial integration acts as a smoothing, except near $\varphi = 0$ where accordingly $I_n(\varphi)$ fluctuates on a much finer scale.

4. Summary, applications and discussion

In this paper we have proposed the representation of eigenfunctions in momentum space as an important and useful complementary picture to the commonly used position representation. In particular, we have introduced the radially integrated momentum distribution $I_n(\varphi)$, which captures all essential features of the momentum distribution $|\hat{\psi}_n(\boldsymbol{p})|^2$. As $I_n(\varphi)$ is just a one-dimensional function, it provides the information on the momentum distribution in a very condensed form. Explicit formulae for $\hat{\psi}_n(\boldsymbol{p})$ and $I_n(\varphi)$, and also the angular integrated momentum distribution $R_n(r)$, are given in terms of the normal derivative $u_n(s)$ along the billiard boundary, which allows for an efficient numerical computation of these quantities.

For the stadium and the cardioid billiard several examples of $|\psi_n(\boldsymbol{q})|^2$, $|\hat{\psi}_n(\boldsymbol{p})|^2$, $I_n(\varphi)$, and $R_n(r)$ are given. For the stadium billiard in particular, the bouncing ball modes lead to significant peaks in the radially integrated momentum densities $I_n(\varphi)$. Also, eigenfunctions showing scarring in position space lead to scarred states in momentum space. In addition to eigenstates showing localization around unstable periodic orbits, we have found for the cardioid billiard examples of eigenfunctions which are localized along cusp orbits, which run into the singularity of the cardioid billiard. Such *diffractive scars* are surprisingly clearly visible, despite the fact that the contribution of the corresponding orbit to the density of states is of lower order in $\hbar$ than the periodic orbits [24]. Our numerical studies also reveal that there are eigenstates for which the correspondence between localization in position space and localization in momentum space is not as clear as one would expect. We see two main reasons for this: firstly, the fluctuations appear to be larger in momentum space than in position space (this is also seen in the results for the rate of quantum ergodicity in momentum space, which appears to be slower than in position space [34]). Secondly, scars which are weak both in position and momentum space are more visible in position space. This is because the usually symmetric pattern of the scar can be detected by the eye more easily against the fluctuating background in the two-dimensional plot of $|\psi_n(\boldsymbol{q})|^2$ than in $|\hat{\psi}_n(\boldsymbol{p})|^2$ or $I_n(\varphi)$.

An application of the radially integrated momentum distribution $I_n(\varphi)$ could be to use it to construct a quantity which detects localized eigenfunctions. A suitable definition might be $I_n^{\text{scar}} := \sum_{\varphi_i} \frac{1}{2\delta l_i} \int_{\varphi_i - \delta}^{\varphi_i + \delta} I_n(\varphi)\,\mathrm{d}\varphi$, where l_i is the geometric length of the orbit segment corresponding to the direction φ_i and δ is some appropriate width, which might be chosen to be energy dependent. In this context it may be also useful to employ the results of the semiclassical studies of eigenfunctions [39–41] to obtain expressions for $I_n(\varphi)$ in terms of periodic orbits. A number of different scar measures have been defined and studied, as, for example, the integral of the Wigner function over a tube around the orbit in phase space [41], the integral over a tube in position space [42], or the use of quantum Poincaré sections [43]: see [44] for a recent review and references therein.

The use of momentum distributions as representations of eigenstates may also be useful for other systems, like systems with potential, etc. The definition of the radially integrated momentum density may easily be generalized to other scaling systems. The usefulness of $I_n(\varphi)$ is due to the fact that the classical motion occurs on straight lines in Euclidean billiards. If this does not hold, the above simple interpretation of $I_n(\varphi)$ is lost.

We believe that the use of momentum distributions, in particular the radially integrated momentum distribution, is a convenient and useful representation, providing additional information to the commonly used position space representation.

Acknowledgments

Appendix. Symmetry reduction

When the billiard has some symmetries they can be used to reduce the domain of integration over the boundary to a smaller part in integrals as (28). We shall discuss as examples the stadium billiard and the cardioid billiard. To simplify the notation we use $q = (x, y)$.

The stadium billiard has two symmetries: it is symmetric with respect to reflection at the x-axis and at the y-axis. Therefore, the eigenfunctions can be choosen to be even or odd with respect to each of these symmetries. So we treat the case of a function $\psi(x, y)$ which satisfies

$$\psi(-x, y) = (-1)^{l_x} \psi(x, y) \tag{40}$$

$$\psi(x, -y) = (-1)^{l_y} \psi(x, y) \tag{41}$$

with $l_x, l_y \in \{0, 1\}$. Thus ψ either satisfies Dirichlet or Neumann boundary conditions on the symmetry axes. The symmetry of the wavefunction now implies certain symmetries of the normal derivative $u(s) = n(s)(\nabla \psi)(q(s))$. Denoting by L the total length of the boundary of the full system, we can express $u(s)$ for $s \in [L/4, L/2]$, $s \in [L/2, 3L/4]$ and $s \in [3L/4, L]$ in terms of $u(s)$ for $s \in [0, L/4]$. Here, we choose $s = 0$ to be the intersection of the horizontal symmetry axis with the right semicircle, and s is oriented counterclockwise. One gets for $s \in [0, L/4]$

$$u(L/2 - s) = (-1)^{l_x} u(s) \tag{42}$$

$$u(L/2 + s) = (-1)^{l_x + l_y} u(s) \tag{43}$$

$$u(L - s) = (-1)^{l_y} u(s). \tag{44}$$

These relations can be used to reduce an integral over the boundary $\int_0^L f(s) u(s) \, ds$ to an integral over one quarter of the boundary. For instance, with (42) one gets

$$\int_{L/4}^{L/2} u(s) f(s) \, ds = \int_{-L/4}^{0} u(L/2 + s) f(L/2 + s) \, ds = \int_0^{L/4} u(L/2 - s) f(L/2 - s) \, ds$$

$$= \int_0^{L/4} (-1)^{l_x} u(s) f(L/2 - s) \, ds \tag{45}$$

and applying (43) and (44) to the other parts of the integral leads to

$$\int_0^L u(s) f(s) \, ds = \int_0^{L/4} u(s)[f(s) + (-1)^{l_x} f(L/2 - s)$$

$$+ (-1)^{l_x + l_y} f(L/2 + s) + (-1)^{l_y} f(L - s)] \, ds \tag{46}$$

which is the desired reduction of the integral. We have to also treat double integrals over the boundary of the form $\int_0^L \int_0^L u(s) \bar{u}(s') f(s, s') \, ds \, ds'$. If we use (46) we get an integral with 16 terms, but for special $f(s, s')$ this can be reduced further. If f is of the form

$$f(s, s') = g(|q(s) - q(s')|) \tag{47}$$

which is the case in our applications, then we have

$$f(s, s') = f(L/2 - s, L/2 - s') = f(L/2 + s, L/2 + s') = f(L - s, L - s'). \tag{48}$$

Because of the symmetry of the billiard the distance between the points on the boundary is the same for all four pairs of arguments of f. Applying (48) and (46) to a double integral over a function of type (47) leads to

$$\int_0^L \int_0^L u(s)\overline{u}(s') f(s, s') \, ds \, ds' = \int_0^{L/4} \int_0^{L/4} u(s)\overline{u}(s') \tilde{f}(s, s') \, ds \, ds' \tag{49}$$

with

$$\tilde{f}(s, s') = 4[f(s, s') + (-1)^{l_x} f(s, L - s') + (-1)^{l_x + l_y} f(s, L/2 + s') \\ + (-1)^{l_y} f(s, L/2 - s')]. \tag{50}$$

The cardioid billiard has only one reflection symmetry at the x-axis, so the eigenfunctions can be chosen to be even or odd,

$$\psi(x, -y) = (-1)^{l_y} \psi(x, y) \tag{51}$$

with $l_y \in \{0, 1\}$. For the normal derivative this leads to

$$u(L - s) = (-1)^{l_y} u(s) \tag{52}$$

and so we get for an integral over the boundary

$$\int_0^L u(s) f(s) \, ds = \int_0^{L/2} u(s)[f(s) + (-1)^{l_y} f(L - s)] \, ds. \tag{53}$$

For a double integral over a function of type (47) one obtains

$$\int_0^L \int_0^L u(s)\overline{u}(s') f(s, s') \, ds \, ds' = \int_0^{L/2} \int_0^{L/2} u(s)\overline{u}(s') 2[f(s, s') \\ + (-1)^{l_y} f(s, L - s')] \, ds \, ds'. \tag{54}$$

References

[1] Berry M V 1977 Semi-classical mechanics in phase space: A study of Wigner's function *Phil. Trans. R. Soc.* A **287** 237–71
[2] Hillery M, O'Connell R F, Scully M O and Wigner E P 1984 Distribution functions in physics: Fundamentals *Phys. Rep.* **106** 121–67
[3] Heller E J 1984 Bound-state eigenfunctions of classically chaotic Hamiltonian systems: Scars of periodic orbits *Phys. Rev. Lett.* **53** 1515–18
[4] Klakow D and Smilansky U 1996 Wavefunctions, expectation values and scars on Poincaré sections—A scattering approach *J. Phys. A: Math. Gen.* **29** 3213–31
[5] Leboeuf P and Voros A 1990 Chaos-revealing multiplicative representation of quantum eigenstates *J. Phys. A: Math. Gen.* **23** 1765–74
[6] Tualle J M and Voros A 1995 Normal modes of billiards portrayed in the stellar (or nodal) representation *Chaos Solitons Fractals* **5** 1085–102
[7] Crespi B, Perez G and Chang S-J 1993 Quantum Poincaré sections for two-dimensional billiards *Phys. Rev.* E **47** 986–91
[8] Riddel R J Jr 1979 Boundary-distribution solution of the Helmholtz equation for a region with corners *J. Comp. Phys.* **31** 21–41
[9] Berry M V and Wilkinson M 1984 Diabolical points in the spectra of triangles *Proc. R. Soc.* A **392** 15–43
[10] Boasmann P A 1994 Semiclassical accuracy for billiards *Nonlinearity* **7** 485–537
[11] Gröbner W and Hofreiter N 1973 *Integraltafel. Zweiter Teil. Bestimmte Integrale* 5th edn (New York: Springer)
[12] Stifter P 1996 Quantenbillards and quantenchaos *PhD Thesis* Abteilung für Quantenphysik, Universität Ulm
[13] Bunimovich L A 1974 On ergodic properties of certain billiards *Funct. Anal. Appl.* **8** 254–5

[14] Bunimovich L A 1979 On the ergodic properties of nowhere dispersing billiards *Commun. Math. Phys.* **65** 295–312
[15] Biham O and Kvale M 1992 Unstable periodic orbits in the stadium billiard *Phys. Rev.* A **46** 6334–9
[16] Bäcker A and Chernov N 1998 Generating partitions for two-dimensional hyperbolic maps *Nonlinearity* **11** 79–87
[17] Robnik M 1983 Classical dynamics of a family of billiards with analytic boundaries *J. Phys. A: Math. Gen.* **16** 3971–86
[18] Wojtkowski M 1986 Principles for the design of billiards with nonvanishing Lyapunov exponents *Commun. Math. Phys.* **105** 391–414
[19] Szász D 1992 On the K-property of some planar hyperbolic billiards *Commun. Math. Phys.* **145** 595–604
[20] Markarian R 1993 New ergodic billiards: exact results *Nonlinearity* **6** 819–41
[21] Prosen T and Robnik M 1994 Private communication
[22] Robnik M 1984 Quantising a generic family of billiards with analytic boundaries *J. Phys. A: Math. Gen.* **17** 1049–74
[23] Prosen T and Robnik M 1993 Energy level statistics in the transition region between integrability and chaos *J. Phys. A: Math. Gen.* **26** 2371–87
[24] Bruus H and Whelan N D 1996 Edge diffraction, trace formulae and the cardioid billiard *Nonlinearity* **9** 1023–47
[25] Bäcker A and Dullin H R 1997 Symbolic dynamics and periodic orbits for the cardioid billiard *J. Phys. A: Math. Gen.* **30** 1991–2020
[26] Dullin H R 1998 Symbolic dynamics and the discrete variational principle *J. Phys. A: Math. Gen.* **31** 9065–72
[27] Shnirelman A I 1974 Ergodic properties of eigenfunctions *Usp. Math. Nauk* **29** 181–2 (in Russian)
[28] Shnirelman A I 1993 On the asymptotic properties of eigenfunctions in the regions of chaotic motion *KAM Theory and Semiclassical Approximations to Eigenfunctions* ed V F Lazutkin (Berlin: Springer)
[29] Zelditch S 1987 Uniform distribution of eigenfunctions on compact hyperbolic surfaces *Duke. Math. J.* **55** 919–41
[30] Colin de Verdière Y 1985 Ergodicité et fonctions propres du laplacien *Commun. Math. Phys.* **102** 497–502 (in French)
[31] Helffer B, Martinez A and Robert D 1987 Ergodicité et limite semi-classique *Commun. Math. Phys.* **109** 313–26 (in French)
[32] Sarnak P 1995 Arithmetic quantum chaos *Israel Math. Conf. Proc.* **8** 183–236
[33] Knauf A and Sinai Ya G (with a contribution by Baladi V) 1997 *Classical Nonintegrability, Quantum Chaos, DMV–Seminar 27* (Basel: Birkäuser)
[34] Bäcker A, Schubert R and Stifter P 1997 Rate of quantum ergodicity in Euclidean billiards *Phys. Rev.* E **57** 5425–47
Bäcker A, Schubert R and Stifter P 1998 *Phys. Rev.* E **58** 5192 (erratum)
[35] Tanner G 1997 How chaotic is the stadium billiard? A semiclassical analysis *J. Phys. A: Math. Gen.* **30** 2863–88
[36] Bäcker A, Schubert R and Stifter P 1997 On the number of bouncing-ball modes in billiards *J. Phys. A: Math. Gen.* **30** 6783–95
[37] Bäcker A 1998 Classical and quantum chaos in billiards *PhD Thesis* Abteilung Theoretische Physik, Universität Ulm
[38] Aurich R, Bäcker A, Schubert R and Taglieber M 1999 Maximum norms of chaotic quantum eigenstates and random waves *Physica* D **129** 1–14
[39] Bogomolny E B 1988 Smoothed wave functions of chaotic quantum systems *Physica* D **31** 169–89
[40] Berry M V 1989 Quantum scars of classical closed orbits in phase space *Proc. R. Soc.* A **423** 219–31
[41] Agam O and Fishman S 1993 Quantum eigenfunctions in terms of periodic orbits of chaotic systems *J. Phys. A: Math. Gen.* **26** 2113–37
Agam O and Fishman S 1993 *J. Phys. A: Math. Gen.* **26** 6595 (corrigendum)
[42] Li B and Hu B 1998 Statistical analysis of scars in stadium billiard *J. Phys. A: Math. Gen.* **31** 483–504
[43] Simonotti F P, Vergini E and Saraceno M 1997 Quantitative study of scars in the boundary section of the stadium billiard *Phys. Rev.* E **56** 3859–67
[44] Kaplan L 1999 Scars in quantum chaotic wavefunctions *Nonlinearity* **12** R1–R40